13 July 2026

Hydrology-Based Evaluation of Irrigation and Cropping Practices in Relation to Malaria Transmission in Western Kenya

Ai-Ling Jiang[1], Ming-Chieh Lee[2], Harrysone Atieli[3], Guiyun Yan[4], Kuo-lin Hsu[5]

1. University of California Irvine Department of Civil and Environmental Engineering
2. Department of Population Health and Disease Prevention, School of Public Health, Susan and Henry Samueli College of Health Sciences, University of California Irvine
3. Tom Mboya University
4. Department of Population Health and Disease Prevention, School of Public Health, Susan and Henry Samueli College of Health Sciences, University of California Irvine
5. University of California, Irvine

Keywords

ParFlow-CLM, Malaria Transmission, Agricultural practices, Food Security, EMOD, Irrigation

Hydrology-Based Evaluation of Irrigation and Cropping Practices in Relation to Malaria Transmission in Western Kenya

Ai-Ling Jiang[1], Ming-Chieh Lee[2], Harrysone Atieli[3], Guiyun Yan[2], Kuolin Hsu[1]

[1]Center for Hydrometeorology and Remote Sensing, Department of Civil and Environmental Engineering, University of California Irvine, Irvine, CA, USA

[2]Department of Population Health and Disease Prevention, School of Public Health, Susan and Henry Samueli College of Health Sciences, University of California Irvine, Irvine, CA, USA

[3]Sub-Saharan International Centre of Excellence for Malaria Research, Tom Mboya University, Homabay, Kenya

Corresponding author: Ai-Ling Jiang (jiangal@uci.edu), Guiyun Yan (guiyuny@uci.edu), Kuolin Hsu (kuolinh@uci.edu)

Key Points:

- A hydrology-based model was created to simulate transmission across various agricultural practices spatially
- Timing and spatial distribution of irrigation determined mosquito larval habitats dynamics more than total irrigation amount
- Human and vector mobility can affect malaria prevalence, especially in water-efficient irrigation settings where transmission is localized

Abstract

Irrigation is widely linked to increased malaria vector population and transmission in rural Africa, yet it remains essential for improving food security. Balancing agricultural productivity with public health therefore requires approaches that consider malaria risk. In this study, we integrated a hydrologic model with an agent-based malaria model to evaluate the impacts of cropping practices, irrigation strategies, and human and mosquito mobility on malaria transmission in Homa Bay, Kenya. We examined scenarios with single crops (either staple or cash crops) and mixed cropping systems, alongside irrigation methods including flood, intermittent, and drip irrigation. The modeling framework captures spatiotemporal dynamics of mosquito breeding habitats driven by crop water demands and irrigation scheduling. Results show that staple crops such as rice required approximately 12% more irrigation than vegetables but were associated with 3-7% lower transmission metrics. This suggests that the timing and spatial distribution of water application are more important than total irrigation volume in determining larval habitat conditions. Combining intermittent and drip irrigation reduced malaria prevalence by 44% relative to flood irrigation, as it limited the extent and persistence of larval habitats. Water-efficient irrigation strategies also concentrated transmission into smaller areas, making targeted interventions more feasible. Under these more heterogeneous risk patterns, human movement and vector dispersal played a critical role in shaping malaria prevalence. Overall, the integrated modeling approach provides a framework for evidence-based agricultural planning that meets crop water demands while reducing malaria risk.

Plain Language Summary

In rural Africa, expanding irrigation helps farmers grow more food and rely less on rainfall, but it can also create mosquito breeding sites that facilitate malaria transmission. Farming practices should therefore support both food production and public health. In this study, we combined a water model with a malaria model to see how cropping practices, irrigation styles and movement of people and mosquitoes affect malaria risk in Homa Bay, Kenya. We tested single and mixed crops, and irrigation options including flooding, intermittent, and drip systems

The results showed that growing rice used 12% more irrigation water than vegetables but transmission metrics were 3-7% lower. This indicates that timing and location of water application matter more than total amount in determining mosquito breeding conditions. The combination of intermittent and drip irrigation reduced malaria transmission by 44% compared to flood irrigation because it limited standing water in fields. These water-efficient irrigation methods also kept malaria transmission more localized, potentially enabling targeted control efforts. In these localized conditions, movement of people and mosquitoes became especially important because infections could spread between high- and low-risk areas. Overall, the combined modeling approach can help guide farming practices that meet water needs while minimizing malaria risk.

1 Introduction

Agriculture remains a cornerstone of economic development in Africa, where reliable water access is essential for crop production and food security (Gracia-de-Rentería et al., 2024). Yet, more than 90% of cultivated land in sub-Saharan Africa is rainfed, leaving agricultural systems highly vulnerable to rainfall variability and climatic extremes (Karpouzoglou & Barron, 2014). Expanding irrigation is widely recognized as a key strategy to improve resilience and sustain productivity (Xie et al., 2020), as it allows farmers to extend growing seasons and stabilize yields. In practice, however, many irrigation schemes fail to deliver these benefits. Despite substantial investments from local governments and international partners, outcomes are often limited by low farmer adoption, inefficient water use, and poor profitability (Higginbottom et al., 2021; Kanda & Lutta, 2022; Nakawuka et al., 2018). Addressing these constraints requires stronger governance, greater farmer engagement, and more effective water management to ensure the long-term sustainability of irrigation initiatives (Merrey et al., 2017; Nakawuka et al., 2018).

Irrigation development also introduces important public health challenges. A key concern is malaria, a water-related vector-borne disease that remains endemic in 83 countries, with over 90% of global cases and deaths occurring in Africa (Haileselassie et al., 2021; Ondeto et al., 2022; Patz et al., 2000; World Health Organization, 2024). In many parts of the region, flood irrigation is the predominant irrigation method due to its simplicity and lower initial cost (Frenken, 2005). However, this approach often leads to inefficient water use and formation of stagnant pools, which provide breeding habitats for *Anopheles* mosquitoes, the primary vector of malaria and increase disease transmission (Djègbè et al., 2020; Mboera et al., 2010).

Integrating malaria prevention into agricultural practices is therefore necessary (Frake et al., 2024; Janko et al., 2018). The World Health Organization (WHO) acknowledged that environmental management can be incorporated into national malaria control programs (World Health Organization, 2023). These approaches focus on modifying or manipulating malaria vector larval habitats to limit their formation and persistence (Walker & Lynch, 2007). For example, intermittent irrigation has been found to introduce dry periods between watering cycles, disrupting larval development and reducing mosquito populations in rice fields (Chan et al., 2022; Djègbè et al., 2020; Keiser et al., 2002; Mutero et al., 2000).

Implementing these strategies effectively requires a comprehensive understanding of how hydrological processes influence mosquito breeding. Modeling tools have become valuable for evaluating such interventions and guiding locally tailored solutions. For instance, Gu and Novak (2009) used an agent-based model to show that removing mosquito larval habitats near human settlements can substantially reduce malaria risk. Similarly, Gianotti et al. (2009) applied hydrologic modeling in Banizoumbou, Niger, to demonstrate that surface modifications, such as leveling and plowing, can reduce the persistence of breeding pools. Other modeling studies have shown that regulating water levels in reservoirs can help reduce shoreline habitats for mosquitoes without compromising hydropower generation or downstream irrigation supply (Kibret et al., 2015; Kibret et al., 2019; Reis et al., 2011).

While these studies highlight the potential of environmental management in controlling malaria, there is limited research on how particular agricultural decisions, particularly cropping

practices and irrigation strategies, influence malaria risk in irrigated landscapes. As irrigation expands to meet growing food demands, understanding the influence of these decisions on malaria vector larval habitats and disease transmission becomes crucial. Such insight is essential for designing integrated approaches that improve agricultural productivity while protecting public health.

This study examines the potential of advanced irrigation strategies, including intermittent and drip irrigation, to reduce malaria transmission in a developing irrigation scheme in Homa Bay, Kenya. We also evaluate malaria transmission under different cropping practice scenarios, comparing staple crops for local food security with cash crops for commercial markets. To perform this assessment, we use a hydrology-based malaria model that integrates the ParFlow-Community Land Model (ParFlow-CLM) (Ashby & Falgout, 1996; Jones & Woodward, 2001; Kollet & Maxwell, 2006; Maxwell, 2013; Maxwell & Kollet, 2008) with the Epidemiological MODeling (EMOD) framework (Bershteyn et al., 2018; Eckhoff, 2011, 2012a, 2012b). This integrated model explicitly simulates surface water pooling as influenced by irrigation frequency, crop water demand, and cultivated area, while also considering human movement and malaria vector dispersal. By capturing the interactions between hydrology, cultivation, and disease transmission, the model allows a detailed assessment of how different agricultural decisions affect vector populations and human malaria risk. To the best of our knowledge, this is the first study to use such a coupled modeling approach to examine irrigation strategies and cropping patterns in relation to malaria transmission in a sub-Saharan agricultural setting.

2 Materials and Methods

2.1 Study Area

The study area encompasses the Oluch irrigation scheme and its vicinity along the shores of Lake Victoria's Winam Gulf in Homa Bay County, western Kenya (Figure 1a). Spanning roughly 170 km², the area comprises both irrigated and non-irrigated lands, with elevations between 1,135 and 1,310 m above sea level. Launched in 2007, the Oluch irrigation project was designed to utilize gravity-fed water from the Awach Tende River for small-scale irrigation. The project involves establishing 53 irrigation blocks and building canals to channel water from the river to agricultural fields (Figure 1b). Its primary goal is to boost food production in the region through its capacity to support the cultivation of maize, rice, vegetables, and other horticultural crops (Omoro, 2018).

The Oluch irrigation scheme experiences a bimodal rainfall pattern (Figure S1), with a long rainy season from March to June and a shorter rainy period from October to November. The long rainy season generally coincides with peak malaria transmission. Mean annual precipitation is approximately 1,351 mm and frequently causes flooding within the irrigation scheme. Based on flood risk exposure, the irrigation scheme was divided into three zones: long-term flooding (two to four weeks of inundation, mainly in April and May), short-term flooding (less than two weeks), and areas unaffected by flooding (GFA Terra Systems et al., 2005) (Figure 1b). All cropping practices and irrigation strategies evaluated in the scenario analyses are applied exclusively within the irrigation scheme.

Homa Bay is a malaria-endemic region with transmission occurring throughout the year. The primary malaria vector is the *Anopheles arabiensis* mosquito, which favors sunlit, stagnant water for breeding (Ondeto et al., 2022; Orondo et al., 2023). In this modeling effort, it was assumed to be the only vector species. Past research has demonstrated a strong association between irrigation and malaria risk in the area, as irrigated areas exhibit higher mosquito densities and more than twice the prevalence of *Plasmodium* infection (Omondi et al., 2022). Furthermore, clinical malaria incidence in irrigated areas has been reported to be nearly three times higher compared to their non-irrigated counterparts (Ondeto et al., 2022; Zhou et al., 2022).

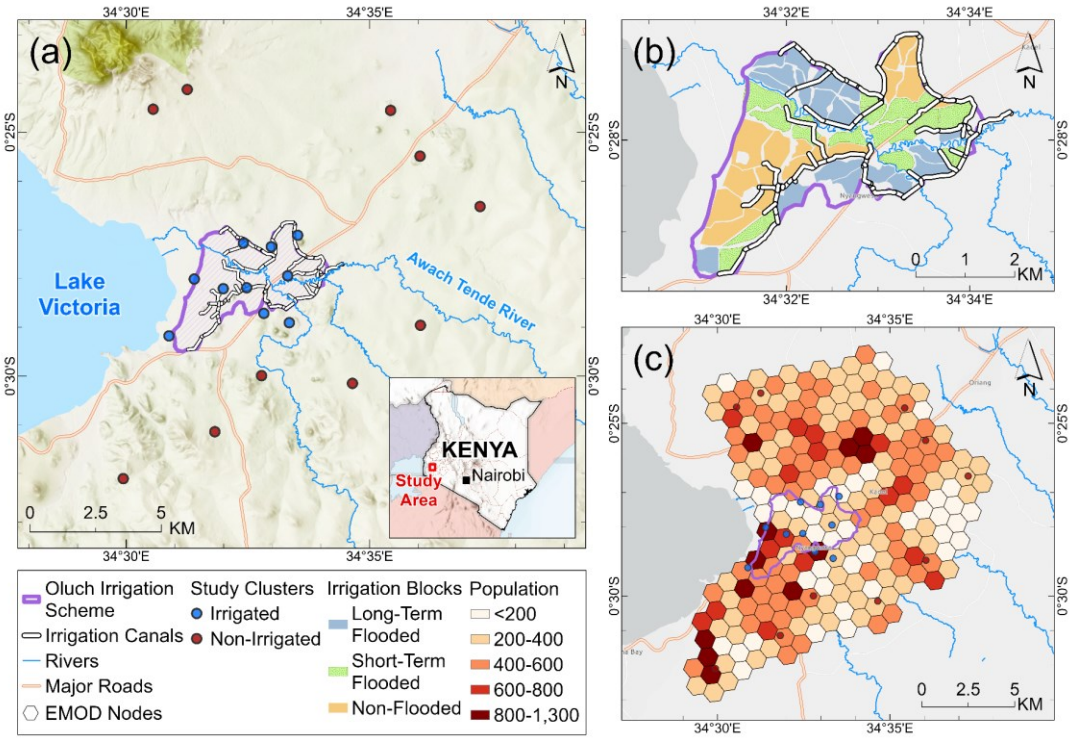

Figure 1. Modeling domain. (a) Study area and the Oluch irrigation scheme. Twenty study clusters (10 in irrigated setting and 10 in non-irrigated setting) were identified to provide field data for model development and calibration. Each cluster covers 1-2.5 km^2 and contains 40-50 households, or approximately 300-500 residents. (b) Irrigation blocks classified by flood conditions. (c) EMOD modeling nodes and associated population distribution.

2.2 Model Domain and Overview

In this study, we employed a hydrology-integrated malaria modeling framework that was previously developed and validated in an Ethiopian irrigated sugarcane plantation (Jiang, Lee, et al., 2023). This framework coupled ParFlow-CLM with EMOD to capture the spatiotemporal variability of larval habitats and resulting malaria transmission dynamics at high resolution.

ParFlow-CLM is a three-dimensional, gridded hydrologic model that simulated terrestrial water cycle processes across the study area. The model domain was discretized at a 90 m

horizontal resolution with five vertical subsurface layers (0.1 m, 0.3 m, 0.6 m, 1 m, and 68 m), yielding a total depth of 70 m from ground surface to bedrock. Subsurface water movement was governed by the Richards' equation (Richards, 1931), while overland flow and its interaction with the subsurface flow were represented by diffusive wave boundary conditions (Kollet & Maxwell, 2006). Land-atmospheric interactions including evapotranspiration and heat fluxes were incorporated based on land use classifications and vegetation canopy properties (Dai et al., 2003). ParFlow-CLM was run at an hourly timestep to resolve hydrologic processes, with surface soil saturation output daily for coupling with EMOD. These daily soil saturation estimates were used to infer larval habitat availability and drive mosquito development in EMOD.

EMOD is an agent-based epidemiological model that simulates interactions among humans, mosquito vectors, and their shared environment using rule-based behaviors defined by agent attributes (Bershteyn et al., 2018). It represents the entire malaria transmission cycle, including human and vector population dynamics, human immunity, within-host parasite dynamics, and intervention effects (Eckhoff, 2013). In this study, EMOD was run at a daily timestep and organized into spatial units ("node") representing local malaria transmission environments. Each node corresponded to an Uber H3 level 8 hexagon (Brodsky, 2018), covering approximately 0.75 km^2. The study area comprised 225 nodes (Figure 1c), with an estimated population of around 88,000 in 2020 (Meta, 2025). Human movement between nodes was modeled using a radiation model based on population size and inter-node distance (Simini et al., 2012), while malaria vector dispersal followed a random walk formation parameterized by daily flight distance and the survival rate of the *Anopheles* mosquito (Thomas et al., 2013). Additional details on human movement and vector dispersal modeling are provided in Section 2.5.

The integration of the two models was achieved by replacing EMOD's internal larval habitat module with habitat area estimates derived from ParFlow-CLM soil saturation outputs. Standing water was assumed to form when surface soil saturation exceeded a calibrated threshold (Jiang et al., 2021). Each ponding event was then classified by its duration into one of four habitat types: non-permissive (less than 15 days), temporary (15-30 days), semi-permanent (30-90 days), or permanent (more than 90 days) (Orondo et al., 2023). The dynamic fractional area of each habitat type within each EMOD node was computed and supplied as input to EMOD. Within EMOD, mosquitoes progress through four life stages: eggs, larvae, immature adults which do not seek bloodmeal or reproduce, and mature adults which seeks bloodmeal and reproduces (Eckhoff, 2011). The habitat area derived from ParFlow-CLM governs the number of eggs that can successfully transition to the larval stage, ultimately determining the number of adult female mosquitoes that emerge, feed, reproduce, and contribute to malaria transmission. Further details on the model coupling process can be found in Jiang, Lee, et al. (2023).

2.3 Data for ParFlow-CLM Development and Calibration

ParFlow-CLM requires climate data to drive its hydrologic processes. Rainfall inputs were obtained from Precipitation Estimation from Remotely Sensed Information using Artificial Neural Networks Dynamic Infrared-Rain Rate (PDIR-Now) dataset (Nguyen et al., 2020), which

was bias-corrected using monthly gauge-fused data from the Global Precipitation Climatology Project (Adler et al., 2003). Additional climate variables, including air temperature, specific humidity, surface pressure, wind speeds, and short-wave and long-wave radiations, were sourced from the fifth generation of the global atmospheric reanalysis by the European Centre for Medium-Range Weather Forecasts (ECMRWF) (Hersbach et al., 2023).

Land surface characteristics were defined using a combination of topographic, land cover, and agricultural information. Topography was derived from the Copernicus GLO-30 global digital elevation model (Airbus, 2020), which was hydro-conditioned to remove noise and fill voids while maintaining terrain integrity (Jiang, Hsu, et al., 2023). Land cover was classified based on annual global land use/land cover maps derived from Sentinel-2 imagery, produced by Esri and Impact Observatory (Karra et al., 2021). Agricultural inputs, including crop types and irrigation practices, were guided by a project-specific irrigation scheme design report (GFA Terra Systems et al., 2003) to ensure they were both manageable within the model and representative of real-world practices. Irrigation requirements were further estimated by the reference evapotranspiration data from the Water Productivity through Open Access of Remotely sensed derived data (WaPOR) database (Food and Agriculture Organization, 2020). Additional implementation details are provided in Section 2.6.

The subsurface was modeled as a multi-layered soil zone above an unconsolidated aquifer. The upper two meters below ground surface were designated as soil, with physical and hydraulic properties sourced from the SoilGrids250m TAXOUSDA data set (Hengl et al., 2017) and SoilKsatDB (Gupta et al., 2020). Below this depth, extending to the bedrock, the subsurface was considered as an unconsolidated aquifer with hydrogeologic properties obtained from GLHYMPS 2.0 (Gleeson et al., 2014). To assess the accuracy of ParFlow-CLM outputs, a satellite-based surface soil moisture product developed by the NASA's National Snow and Ice Data Center (Lakshmi & Fang, 2023) was used for benchmarking. A complete list of input and calibration datasets can be found in Table S1.

2.4 Data for EMOD Malaria Model Development and Calibration

Demographic data, climate variables, mosquito ecology, and intervention information were used to characterize agent properties and interactions in EMOD. The initial human population distribution was defined using high-resolution density maps developed by Meta and the Center for International Earth Science Information Network (CIESIN) at Columbia University (Meta, 2025). Land surface temperature data were sourced from the global atmospheric reanalysis dataset provided by ECMWF (Hersbach et al., 2023) to inform temperature-dependent processes such as mosquito development and parasite sporogony.

To estimate the spatial distribution of adult mosquitoes emergence, larval habitat information was compiled from field campaigns conducted during both dry and rainy seasons between 2017 and 2023 (Orondo et al., 2023). A total of 12,977 natural larval habitats were surveyed within 200 m of the edge of the study clusters. (Figure S2). Each habitat was classified by surface water persistence into temporary, semi-permanent, or permanent types, with approximately 20%, 65%, and 15% of habitats falling into each respective category. At each habitat, larvae were sampled using a 350 mL dipper in accordance with the WHO standard

protocol. These data were used to calculate larval density, which was scaled using a calibrated factor to determine larval capacity (Jiang, Lee, et al., 2023) (Table S2). The spatial distribution of larval capacity was interpolated from cluster locations using the Voronoi Diagram method (Aurenhammer, 1991) (Figure S3). This method partitioned the EMOD modeling domain into regions based on proximity to study clusters, so that each region contained all EMOD nodes closest to a given cluster. Nodes within the same region shared the larval capacity of the associated cluster, and these values were multiplied by the derived habitat area from ParFlow-CLM to estimate the maximum number of mosquito larvae that could potentially coexist within each EMOD node.

In addition to the larval habitat survey, entomological and epidemiological indicators were sourced from previous studies (Omondi et al., 2022; Ondeto et al., 2022) to support model calibration. Details of these datasets are provided in Text S1 and the spatiotemporal resolution of all input and calibration data is summarized in Table S3.

2.5 Inter-Node Connectivity in EMOD

In this study, we extended our previous hydrology-integrated malaria modeling framework (Jiang, Lee, et al., 2023) by shifting from a single-node setup to a multi-node simulation, allowing a more realistic representation of spatial heterogeneity in malaria transmission. This enhancement involved establishing connections between nodes to account for both human and mosquito mobility. In EMOD, both human and mosquito mobility are modeled through daily probabilities that individuals can move from one node to another. These probabilities are organized into a square mobility matrix of size N by N, where N is the total number of nodes. Each element in the matrix indicates the probability of movement from a specific origin node to a particular destination node.

2.5.1 Human Movement

To generate the human mobility matrix, we employed a modified radiation model (De Lellis et al., 2021; Simini et al., 2012), which estimated movement based on population and distance data and involves only a single parameter (α). For simplicity, we assumed (1) mobility flows between nodes remain constant over time, and (2) the daily return probability is 0.95, meaning individuals are highly likely to return to their origin nodes in the following day. These assumptions help maintain the population distribution and stabilize movement dynamics. The probability of movement from node i to j, denoted as P_{ij} is defined as

$$P_{ij} = \frac{{n_i}^m r_{ij}}{n_i}, \quad (1)$$

where n_i is the population in node i, ${n_i}^m$ is the mobile subpopulation (individuals capable of migration), and r_{ij} is the probability that a mobile individual from node i chooses node j as the destination.

The mobile subpopulation ${n_i}^m$ was determined using the parameter α, adapted from De Lellis et al. (2021), as follows:

$$n_i{}^m = (1-\alpha)n_i. \quad (2)$$

In the original context, α was used to represent environmental constraints on mobility. Here, it simply indicates the proportion of people who cannot undertake overnight trips. In the absence of detailed local mobility survey, we assumed a uniform α value across all nodes and calibrated it to match an average of 1.65 overnight trips per person over a six-month period, based on survey data from Camlin et al. (2019).

The destination probability r_{ij} considers individuals' tendency to prefer more populated destinations, which acts as a proxy for available opportunities, while also accounting for the distance from the origin and the presence of intervening opportunities (De Lellis et al., 2021). It is calculated as

$$r_{ij} = \begin{cases} \frac{n_i n_j}{(n_i+s_{ij})(n_i+n_j+s_{ij})}, & \text{if } i \neq j, \\ \frac{n_i}{\sum_{l=1}^{N} n_l}, & \text{if } i = j. \end{cases} \quad (3)$$

In this context, s_{ij} denotes the total population within a radius around node i equal to its distance to node j, excluding the populations of nodes i and j. This term encapsulates the concept of intervening opportunities, which affect the attractiveness of a movement destination. Based on this model, the estimated spatial distribution of the initial population in 2014 is presented in Figure 2.

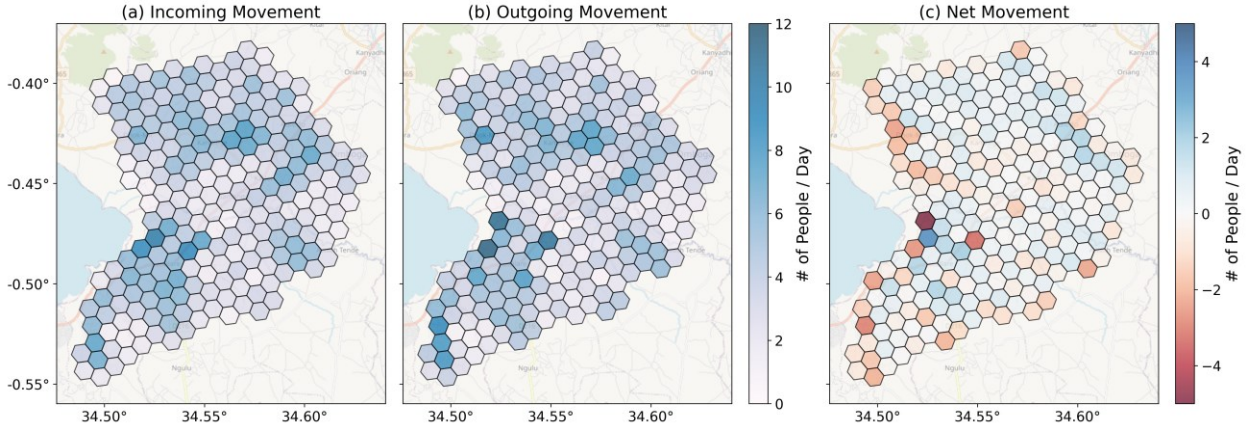

Figure 2. Estimated spatial distribution of human daily movement in 2014 derived from the modified radiation model. (a) Incoming daily movement population, (b) outgoing daily movement population, and (c) net daily movement population, which was calculated as the difference between incoming and outgoing populations.

2.5.2 Malaria Vector Dispersal

Malaria vector dispersal was simulated using a random walk framework following Leung et al. (2022) and Thomas et al. (2013). In the simulation, 10,000 *Anopheles arabiensis* mosquitoes were released from a single origin and their positions were tracked at daily intervals. Each mosquito was assigned an average daily flight distance of 1,040 m (Verdonschot & Besse-Lototskaya, 2014) and a daily survival probability of 0.8 (Atieli et al., 2023; Ntabaliba et al., 2023). At each daily timestep, mosquitoes moved in a random direction, and a subset was

removed according to the survival probability. The simulation continued until all mosquitoes had perished or 40 days was reached, whichever occurred first. The resulting spatial distribution of mosquito endpoints is shown in Figure 3a.

The simulated endpoint locations were aggregated into 100-m displacement bins to estimate mosquito density as a function of distance from the release point. Several commonly employed dispersal distribution functions, including the negative exponential, half-Cauchy, power-law, and Weibull distributions (Cousens et al., 2008) were evaluated for goodness of fit. The Weibull distribution provided the best fit (Figure 3b) and was therefore used to construct a normalized malaria vector dispersal kernel (Figure 3c). This kernel was then integrated over the spatial extent of each destination node to derive the daily probability of mosquito movement from an origin node to that node. Since the kernel is distance-dependent, movement probabilities decrease with increasing distance from the origin. For each origin node, probabilities across all destination nodes, together with the probability of remaining at the origin, were normalized to sum to 1, yielding a distance-dependent, node-to-node mobility matrix consistent with the EMOD spatial framework.

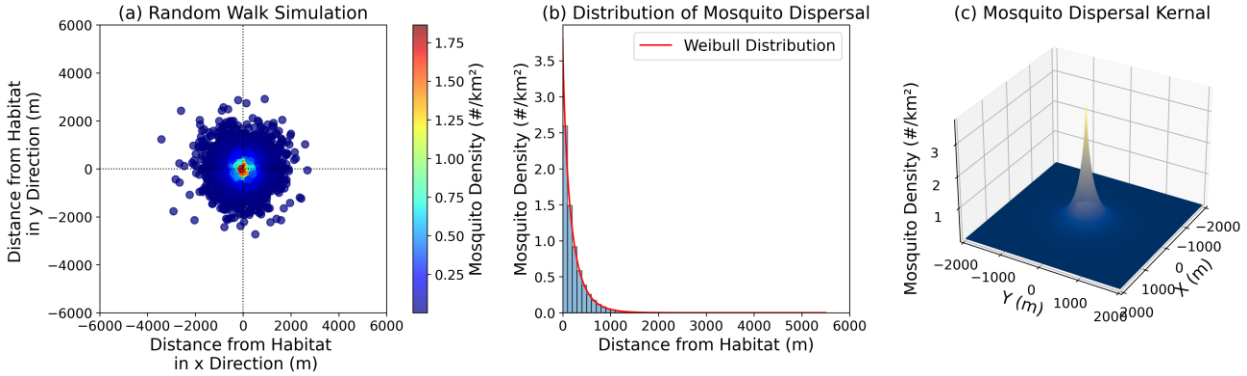

Figure 3. Estimation of adult vector dispersal. (a) End locations of simulated *Anopheles arabiensis* mosquitoes in the random walk framework. (b) Histogram of vector density by displacement from the source location with the fitted Weibull function. (c) Normalized Malaria vector dispersal kernel derived from the fitted Weibull distribution.

2.6 Agricultural Configuration

The hydrology-integrated malaria model was calibrated for the period 2014-2023. ParFlow-CLM was initialized with a 10-year spin-up using the same input data as the calibration period, while EMOD employed a 40-year intervention-free spin-up generated by repeating the same 10-year input sequence to establish stable initial conditions.

The Oluch irrigation scheme includes a mix of irrigated and non-irrigated areas, with flood irrigation as the dominant practice (Ouma et al., 2024). Farmers cultivate a diverse range of crops, including rice, maize, beans, tomatoes, and leafy vegetables such as kale. While farming is largely subsistence-based, many households sell high-value crops in local markets for additional income (Onyango, 2023). Crop production generally follows two rainfall-driven seasons from March to August and from September to February (Food and Agriculture Organization, 2021; Makone et al., 2021; Osika et al., 2023).

For the calibration run, the irrigated areas were configured as expanding from 5% in 2014 to 50% in 2023, with new plots added annually near canals and water sources to approximate gradual infrastructure development (Ouma et al., 2024) (Figure S4). Cropping patterns were assigned based on flood-risk zones defined in the Oluch irrigation scheme design report (GFA Terra Systems et al., 2003) (Figure 1b). In the long-term flooded zone, rice cultivation was grown during the long rains, followed by beans and peas during the short rains to improve soil fertility. In the short-term flooded zone, flood-sensitive crops like vegetables were excluded during the long rains due to the risk of flooding. The non-flooded zone was considered suitable for most crops except rice. These rules defined the spatially and seasonally varying cropping patterns in the model (Figure S5).

Irrigation in ParFlow-CLM was modeled by prescribing irrigation rates for land cover types identified as irrigated. Each land cover type was linked to a specific Plant Functional Type (PFT), characterized by structural and biological parameters that govern surface water balance and evapotranspiration (Gillison, 2016). Since the default cropland category in ParFlow-CLM is not crop-specific, we added land cover types for individual crops and adjusted their PFT parameters accordingly (Table S4).

The theoretical irrigation requirements (Irr) was defined as the difference between crop evapotranspiration (ET_c) and effective precipitation (P_e) (Allen et al., 1998):

$$Irr = ET_c - P_e, \tag{4}$$

where ET_c represents the water demand for crop growth under optimal agronomic and soil moisture conditions. ET_c was estimated as:

$$ET_c = ET_0 \times K_c. \tag{5}$$

Here, ET_0 is the reference evapotranspiration from a well-watered grass surface, and K_c is a crop coefficient that varies by crop type and growth stage (Table S5). In the model, irrigation rates were prescribed directly as ET_c, with irrigation applied only when soil moisture was below full saturation, effectively accounting for the contribution of P_e. Since ET_0 data (Food and Agriculture Organization, 2020) was provided on a monthly basis, irrigation rates were specified monthly and applied uniformly as an average hourly rate throughout each month.

2.7 Model Calibration Procedure

Calibration of the hydrology-integrated malaria modeling framework was conducted in two stages. The first stage focused on the hydrologic component by tuning ParFlow-CLM parameters to improve soil saturation simulations and identifying a soil saturation threshold above which model grid cells were identified as potential larval habitats. The second stage involved calibrating EMOD parameters to improve the accuracy of simulated malaria transmission dynamics.

ParFlow-CLM is a fully integrated, physically based hydrologic model that has demonstrated reliable performance with minimal parameter adjustment (Poméon et al., 2020; Saadi et al., 2022). Due to its computational cost and established robustness, manual calibration was performed on key soil parameters such as saturated hydraulic conductivities.

Model performance was evaluated by comparing the spatial average of simulated surface soil saturation against SMAP-derived soil moisture data (Lakshmi & Fang, 2023).

To further evaluate the spatial accuracy of simulated soil saturation and identify the soil saturation threshold, we calculated the predicted-to-expected (P/E) ratio (Boyce et al., 2002). This ratio tests whether model grid cells with higher simulated soil saturation contain more observed larval habitats than expected by chance. In this analysis, simulated soil saturation values were divided into partially overlapping bins using a moving window approach (Hirzel et al., 2006). For each bin, the P/E ratio was calculated, where *P* represents the proportion of observed larval habitats located in model grid cells whose simulated soil saturation falls within the bin and *E* is the proportion of grid cells in the study area with simulated soil saturation exceeding the midpoint of the bin.

The resulting P/E ratios across bins were used to construct a P/E curve with a 95% confidence interval. The soil saturation threshold was defined as the lowest saturation value for which the lower confidence bound exceeded 1, indicating that observed larval habitats occurred more frequently than expected by random chance in grid cells with soil saturation above this value. The Continuous Boyce Index (CBI) was also calculated to evaluate the monotonicity of the P/E curve (Boyce et al., 2002; Hirzel et al., 2006). A consistently increasing curve indicates strong predictive performance, whereas a flat curve suggests the model performs no better than random (Boyce et al., 2002).

In the second stage, EMOD was calibrated to align model outputs with observed malaria indicators, including adult mosquito density, entomological inoculation rate (EIR), and parasite prevalence. Calibration was performed in two steps using the Gradient Ascent method (Ruder, 2016), which maximizes an objective function by iteratively adjusting model parameters in the direction of steepest ascent. The first step focused on vector dynamics parameters including habitat larval capacity and temperature-dependent growth rates (Table S6). This process was guided by a weighted combination of objective functions, including (1) the correlation between simulated and field adult vector abundance, and (2) the root mean squared error (RMSE) between simulated and observed EIR. In the second step, parameters related to parasite prevalence and malaria incidence (Table S7) were optimized. The objective function was a binomial log-likelihood function which compared the simulated infection prevalence against the observed parasite prevalence. This two-step calibration strategy decouples the entomological and epidemiological components, allowing for targeted tuning and improved model fidelity. Prior to calibration, a sensitivity analysis was conducted to identify parameters with the greatest influence on model outputs.

2.8 Model Scenarios

After calibration, the coupled modeling framework was used to simulate four groups of scenarios designed to isolate the effects of irrigation expansion, cropping patterns, irrigation strategies, and mobility on malaria transmission. The scenario configurations are summarized in Table 1.

The first group represented a baseline scenario in which the 2023 agricultural configuration was maintained for an additional 10 years using historical climate data.

Diversified cropping patterns and flood irrigation over approximately 50% of the scheme remained unchanged, reflecting the status quo of current agricultural practices. This scenario provided a reference for assessing the effects of expanding irrigation.

The second group examined alternative cropping practices under full irrigation coverage using flood irrigation. Three cropping configurations were considered: (1) diversified cropping, which reflected existing practice and includes maize, rice, vegetables, and beans; (2) cash crop dominant, in which vegetables were grown in both crop periods to represent an intensive production strategy focused on profitability; and (3) staple crop dominant, which planted rice during the first crop period followed by maize during the second, consistent with food security objectives.

The third group explored alternative irrigation strategies under full irrigation coverage with diversified cropping practices. Three irrigation configurations were implemented: (1) flood irrigation, reflecting the current condition; (2) intermittent irrigation, applied to rice and bean/pea systems in the long-term flooded zone; and (3) water saving irrigation, which combined intermittent irrigation in flooded zones with conceptual drip irrigation in short-term and non-flooded zones. In the intermittent irrigation configuration, the irrigation threshold was reduced to 90% soil saturation, resulting in longer intervals between irrigation events and a 50% decrease in water use. Drip irrigation was implemented conceptually following Pool et al. (2021), in which model grid cells within the irrigation scheme were partitioned into wet and dry fractions. Wet fractions were irrigated as in the flood method, whereas dry fractions were treated as unirrigated grassland.

The fourth group evaluated the sensitivity of malaria transmission to changes in human and vector mobility under different irrigation strategies. Building on the third group, mobility parameters were perturbed one factor at a time while holding the other constant. These perturbations represented plausible variability in mosquito dispersal and human travel behavior, which could change in response to environmental conditions, habitat distribution, and agricultural activities associated with irrigation (Lutambi et al., 2013; Pindolia et al., 2012; Verdonschot & Besse-Lototskaya, 2014). Human movement scenarios included (1) high movement and (2) low movement, corresponding to half and twice the baseline travel frequencies (0.825 and 3.3 trips per six months). Vector dispersal scenarios included (3) high dispersal and (4) low dispersal, corresponding to half and twice the baseline daily vector flight range (520 m and 2,080 m). Each mobility perturbation was applied to all three irrigation configurations. Spatial patterns and parameter settings for the mobility scenarios are provided in Figures S6 and S7.

Table 1. Configuration of model scenario groups used to evaluate the impacts of cropping practices, irrigation strategies, and mobility on malaria transmission.

Scenario Group	Model Scenario	Irrigated Area	Crops	Irrigation (LT / ST / NF*)	Human Movement	Vector Dispersal
G1: Status Quo	Baseline	50%	Maize, Rice, Vegetables, Beans**	Flood / Flood / Flood	Medium	Medium

G2: Cropping Practice	Diversified Crop Cash Crop Dominant Staple Crop Dominant	100%	Maize, Rice, Vegetables, Beans** Vegetables (both periods) rice in 1st crop period; 100% maize in 2nd crop period	Flood / Flood / Flood	Medium	Medium
G3: Irrigation Strategy	Flood Irrigation Intermittent Irrigation Water Saving Irrigation	100%	Maize, Rice, Vegetables, Peas**	Flood / Flood / Flood Intermittent / Flood / Flood Intermittent / Drip / Drip	Medium	Medium
G4: Irrigation and Mobility Sensitivity* **	High Human Movement Low Human Movement High Vector Dispersal Low Vector Dispersal	Same as G3	Same as G3	Same as G3	High Low Medium Medium	Medium Medium High Low

Notes:
*LT, ST, and NF denote long-term flooded, short-term flooded, and non-flooded zones within the irrigation scheme.
**See Figure S5 for the cropping schedule.
***Each mobility scenario in this group was simulated across the three irrigation strategies defined in G3.

3 Results

3.1 Calibration Results and Performance Assessment

The performance of ParFlow-CLM was evaluated by comparing simulated daily domain-averaged soil saturation to SMAP-derived soil moisture data (Lakshmi & Fang, 2023) from 2017 to 2022. As shown in Figure S8, the simulated values generally agree with the SMAP data in both temporal variability and overall magnitude, yielding a correlation coefficient of 0.66 and a RMSE of 0.038 m^3/m^3. The moderate correlation reflects a tendency for the SMAP data to report lower soil moisture than ParFlow-CLM during dry and cold seasons. This discrepancy likely arises from uncertainties in the downscaling procedure utilized to generate the SMAP data, as well as known reductions in SMAP retrieval accuracy during extremely wet or dry periods, cold months, and in regions with dense vegetation or complex terrain (Fang et al., 2024) . Despite these factors, the correlation is satisfactory and indicates that ParFlow-CLM captures the main soil moisture dynamics.

A predicted-to-expected (P/E) analysis was used to assess how well simulated soil saturation identified potential larval habitat locations. As shown in Figure 4, P/E ratios increased with soil saturation, indicating that observed larval habitats occurred more frequently in areas with higher soil saturation than expected by chance. This pattern was supported by a high Continuous Boyce Index (CBI = 0.95), reflecting strong agreement between simulated soil saturation and observed larval habitat locations. Based on the P/E curve, a soil saturation threshold of 0.91 was selected, where the lower bound of the 95% confidence interval exceeded 1. This threshold was subsequently applied in EMOD simulations to determine grid cells as potential larval habitats.

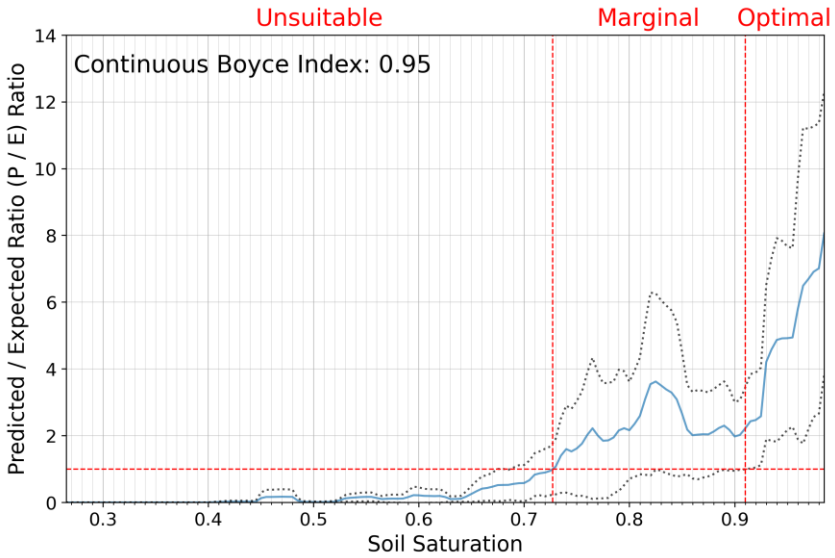

Figure 4. Curve of predicted frequency over expected frequency (P/E) ratio against soil saturation. The black dashed lines demarcate the lower and upper boundaries 95% confidence interval. The horizontal red dashed line with P/E of 1 represents a completely random model that predicts habitats by chance. The P/E curve and its confidence interval were used to define the boundaries of ponding suitability levels (vertical red dashed lines), whereby soil saturation less than 0.73 is unsuitable, between 0.73 and 0.91 is marginal and above 0.91 is optimal.

The EMOD model was assessed by comparing simulated adult vector density, annual EIR, and malaria prevalence with field observations (Omondi et al., 2022; Ondeto et al., 2022) from irrigated and non-irrigated clusters between 2019 and 2023. In 2019, the simulated annual EIR in irrigated clusters (0.34 infectious bites per person per year, ib/p/year) closely matched the observed value (0.35 ib/p/year) (Table S8). In non-irrigated clusters, the model estimated an EIR of 0.077 ib/p/year, slightly higher than the observed value of zero. This difference is acceptable, as EIR measurements in low-transmission settings are often based on very limited observations, leading to high uncertainty and variability in annual estimates.

For adult vector density and malaria prevalence (Figure 5), the model generally reproduced the seasonal patterns and long-term trends. However, it did not capture the sharp increase in prevalence observed in 2022 across both cluster types. This may be due to underestimated rainfall in the satellite-derived climate forcing, which could limit breeding site availability or mosquito survival in the model. Overall, the performance of the EMOD model is

consistent with key transmission patterns observed in the field, providing a calibrated basis for subsequent scenario analyses.

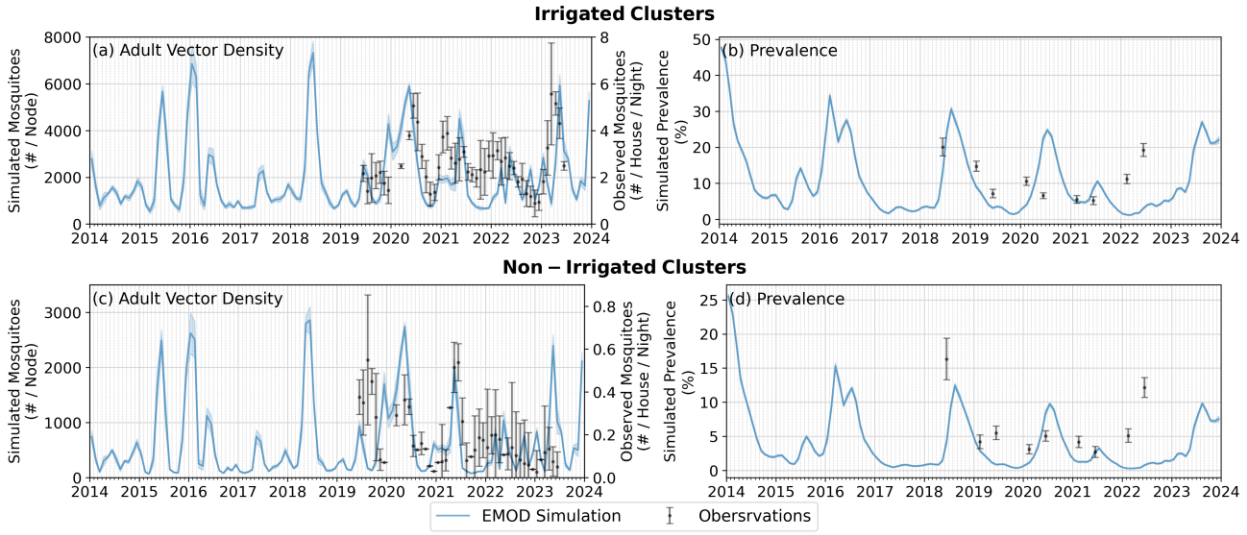

Figure 5. Comparison of simulated adult vectors and malaria prevalence against observation for (a)(b) irrigated clusters and (c)(d) non-irrigated clusters.

3.2 Effect of Cropping Practices on Malaria Transmission

Table 2 shows that fully irrigated conditions (100% irrigation) increased the annual average larval habitat area by 1.93-2.12 times relative to the baseline (50% irrigation), depending on cropping pattern. This expansion corresponded to higher EIR reflecting enhanced vector breeding conditions and increased vector-host contact. In contrast, malaria prevalence increased more modestly, suggesting a dampening effect from acquired immunity. Daily mean profiles over the simulation period showed that habitat expansion was greatest during the dry season (Figure 6c). A lagged response was observed, with EIR rising shortly after the increase in habitat availability (Figure 6b), followed by a delayed increase in prevalence (Figure 6d).

Among the cropping practice scenarios, the cash crop dominant scenario produced the highest larval habitat area, EIR, and malaria prevalence (Table 2). Although the staple crop scenario required the greatest irrigation volume, it did not result in the highest transmission metrics. In this scenario, rice cultivation from March to August coincided with the long rainy season (Figure 6a), when soil was already saturated early in the season. As a result, additional irrigation contributed minimally to further habitat formation. This indicates that the timing of irrigation played a more important role than total irrigation volume in shaping transmission outcomes, particularly in flat farmland with semipervious to impervious soils where drainage was limited once saturation was reached.

Spatial allocation of irrigation further differentiated outcomes across scenarios. Despite similar total irrigation volumes, the cash crop dominant scenario generated 9.8% more larval habitat area than the diversified crop scenario, resulting in 33% higher EIR and 13% higher prevalence. This difference arose from how irrigation was distributed. In the diversified crop scenario, a larger share of irrigation was applied to long-term flooded zones to support water-

intensive rice cultivation (Figure S9a), where persistent inundation limited additional habitat expansion (Figure S9c). In contrast, the cash crop dominant scenario allocated more irrigation to non-flooded and short-term flooded zones, where habitat availability remained sensitive to irrigation inputs. The higher EIR and prevalence in the cash crop dominant scenario corresponded to increased irrigation in these non-flooded and short-term flooded zones.

Table 2. Mean annual (a) irrigation quantity, (b) EIR, (c) larval habitat area, and (d) malaria prevalence in the irrigation scheme under the baseline and different crop practice scenarios. Values in parentheses are ratios relative to the baseline.

Model Scenario	Irrigation Quantity (mm per year)	Habitat Area (average % in the irrigation scheme)	EIR (infectious bites per person per year)	Prevalence (%)
Baseline	423 (1.00)	45.9 (1.00)	1.94 (1.00)	12.8 (1.00)
Diversified Crop	807 (1.91)	88.4 (1.93)	3.42 (1.76)	19.5 (1.52)
Cash Crop Dominant	808 (1.91)	97.4 (2.12)	4.55 (2.35)	22.2 (1.73)
Staple Crop Dominant	905 (2.14)	93.4 (2.03)	4.23 (2.18)	21.4 (1.67)

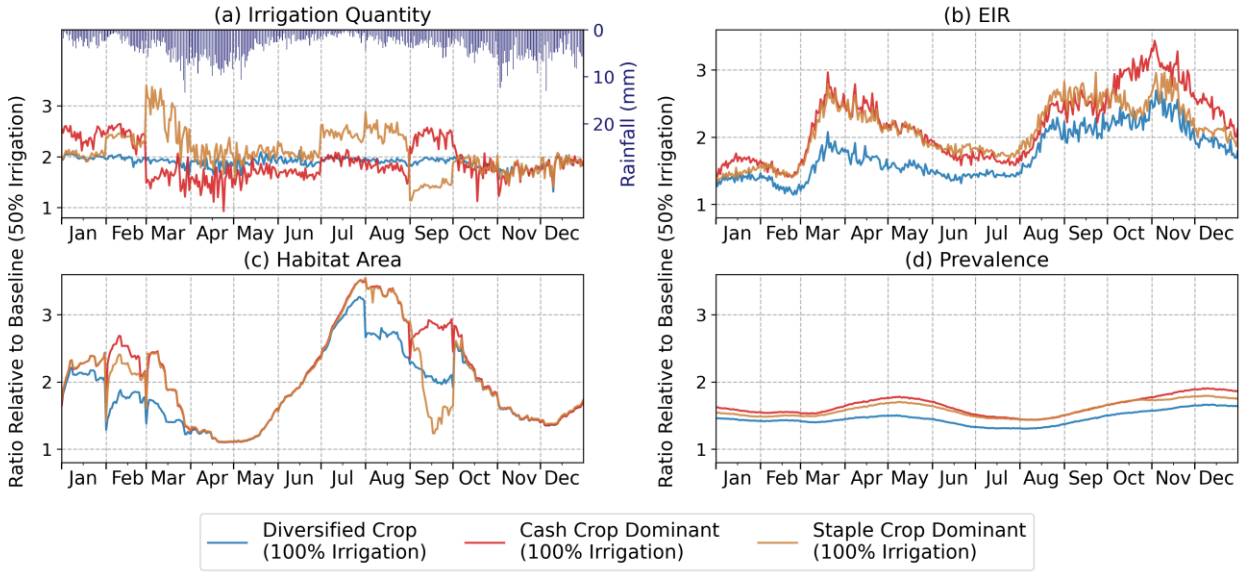

Figure 6. Ratio of 10-year daily mean (a) irrigation quantity, (b) EIR, (c) larval habitat area, and (d) malaria prevalence in the irrigation scheme, for diversified crop, cash crop dominant and staple crop dominant scenarios relative to the baseline.

3.3 Effect of Irrigation Strategies on Malaria Transmission

While expanding irrigation coverage from 50% to 100% increased habitat area by 93%, EIR by 76%, and malaria prevalence by 52% (Table 2), replacing flood irrigation with more efficient methods reduced these impacts. Applying intermittent irrigation to seasonally cultivated rice-bean/pea fields (33% of the irrigated area) reduced habitat area, EIR, and prevalence to 77%, 77%, and 83%, respectively, relative to flood irrigation (Table 3). In the water saving irrigation scenario, intermittent irrigation in these fields was combined with drip irrigation for the remaining crops (67% of the irrigated area), further reducing habitat area, EIR, and prevalence to 47%, 45%, and 56%, respectively.

Reductions were most pronounced during the dry season, when rainfall was limited and irrigation became the dominant source of surface water (Figure 7). Under flood irrigation, persistent surface water supported widespread larval habitats across all zones. In contrast, intermittent irrigation introduced drying intervals that interrupted habitat continuity in the rice-bean/pea fields, while drip irrigation minimized surface pooling by delivering water directly to the plant root zone. These changes in water distribution patterns reduced larval habitat persistence and vector abundance, resulting in lower EIR and prevalence. Relative to flood irrigation, EIR decreased by up to 55%, compared to a 44% reduction in malaria prevalence, indicating a stronger influence on EIR than on malaria prevalence. This difference is consistent with the more immediate response of mosquito dynamics to aquatic habitat availability and the slower response of human infections due to immunity and infection duration.

Table 3. Mean annual (a) irrigation quantity, (b) EIR, (c) larval habitat area, and (d) malaria prevalence in the irrigation scheme under different irrigation strategy scenarios. Values in parentheses are ratios relative to the flood irrigation scenario.

Model Scenario	Irrigation Quantity (mm per year)	Habitat Area (average % in the irrigation scheme)	EIR (infectious bites per person per year)	Prevalence (%)
Flood Irrigation	807 (1.00)	88.4 (1.00)	3.42 (1.00)	19.5 (1.00)
Intermittent Irrigation	670 (0.83)	68.4 (0.77)	2.63 (0.77)	16.2 (0.83)
Water Saving Irrigation	441 (0.55)	41.9 (0.47)	1.54 (0.45)	11.0 (0.56)

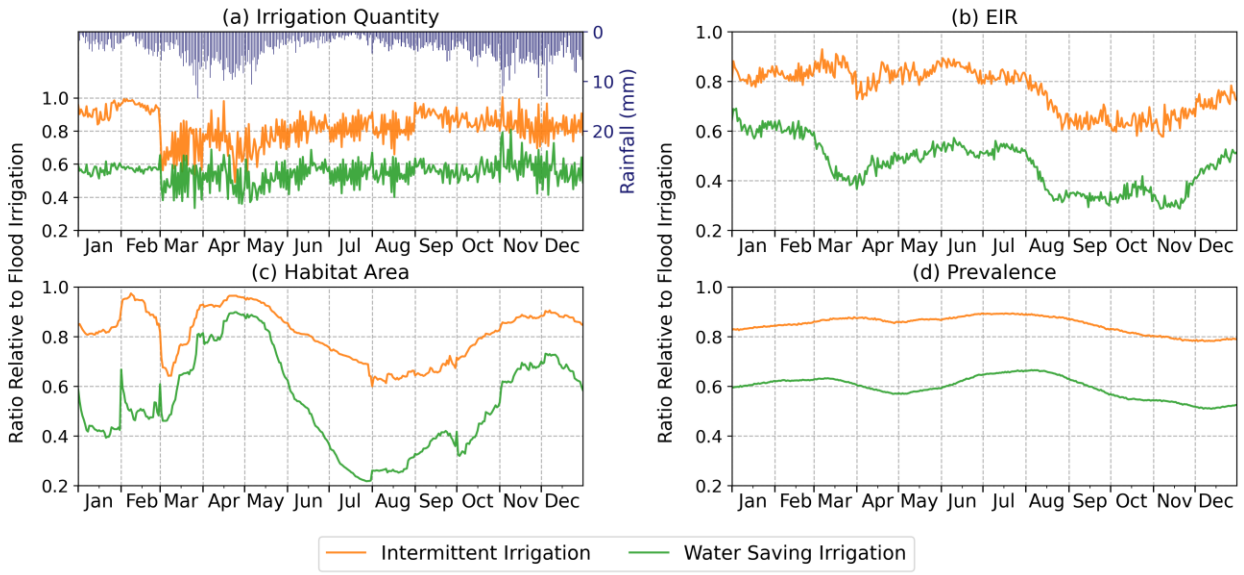

Figure 7. Ratio of 10-year daily mean (a) irrigation quantity, (b) EIR, (c) larval habitat area, and (d) malaria prevalence in the irrigation scheme, for intermittent and water saving irrigation scenarios relative to the flood irrigation scenario.

3.4 Spatial Influence of Irrigation Strategies and Human-Vector Movement on Malaria Transmission

Across all irrigation strategies, adult vector density decreased with distance from the irrigation scheme (Figure 8a-c). Although Malaria prevalence showed a similar spatial decline (Figure 8d-f), it was modulated by human population density (Figure 1c). At comparable vector densities, areas with lower population density exhibited higher prevalence, reflecting greater exposure per individual. Compared to flood irrigation, intermittent irrigation reduced the extent and intensity of transmission hotspots, which were further reduced in the water saving irrigation scenario, with effects extending well beyond the immediate farmland. These strategies curtailed the development of larval habitats, resulting in a more localized distribution of adult mosquitoes and transmission.

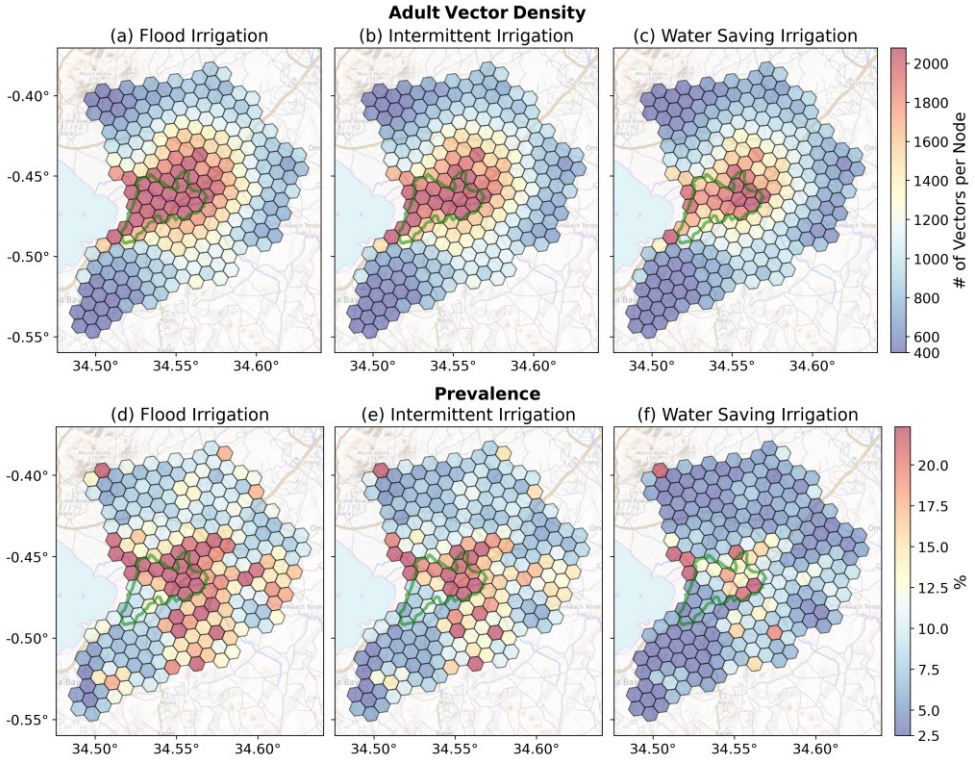

Figure 8. Spatial distribution of (a)(b)(c) annual adult vector density and (d)(e)(f) annual prevalence for each irrigation strategy scenario. The irrigated area was demarcated in green.

To examine the effects of human and vector mobility under different irrigation strategies, EMOD nodes were grouped into four zones based on their distance from the irrigation scheme: 0 km (irrigation scheme), 0-2.5 km, 2.5-5 km, and 5-7.5 km (Figure S10). In the low vector dispersal scenario, adult vector density within the irrigation scheme was higher than in the median (original) setting, with effects diminishing with distance and transitioning to lower densities in the outer zones (Figure S11a-d). In contrast, the high vector dispersal scenario produced lower vector density within the irrigation scheme and higher density in more distant areas. This spatial redistribution was most pronounced under flood irrigation, where greater larval habitat availability within the irrigation scheme supported larger mosquito

populations moving between zones. Malaria prevalence followed similar spatial gradients. Compared to the median setting, the low vector dispersal scenario resulted in higher prevalence across all zones, whereas the high vector dispersal scenario produced lower prevalence, with both effects weakened with distance from the irrigation scheme (Figure 9a-d). Within each zone, the changes in prevalence were greatest under water saving irrigation, where the limited and uneven distribution of breeding sites made transmission highly dependent on mosquito movement.

Changes in human movement did not affect adult vector density but altered malaria prevalence across all zones (Figure 9e-h). Compared to the median setting, the high human movement scenario resulted in higher malaria prevalence, whereas the low human movement produced lowered prevalence. Unlike changes in mosquito dispersal, which redistributed prevalence spatially, changes in human movement produced more spatially uniform responses across zones. This reflects the ability of human movement to connect populations beyond the limited flight range of mosquitoes, allowing infections to spread across zones regardless of local habitat conditions. The influence of human movement on prevalence was greatest under water saving irrigation, followed by intermittent and flood irrigation (Figure 9e). Under water saving irrigation, lower transmission intensity increased the influence of infections introduced through human movement, whereas under flood irrigation, consistently high mosquito-human contact diminished the relative contribution of movement-driven transmission.

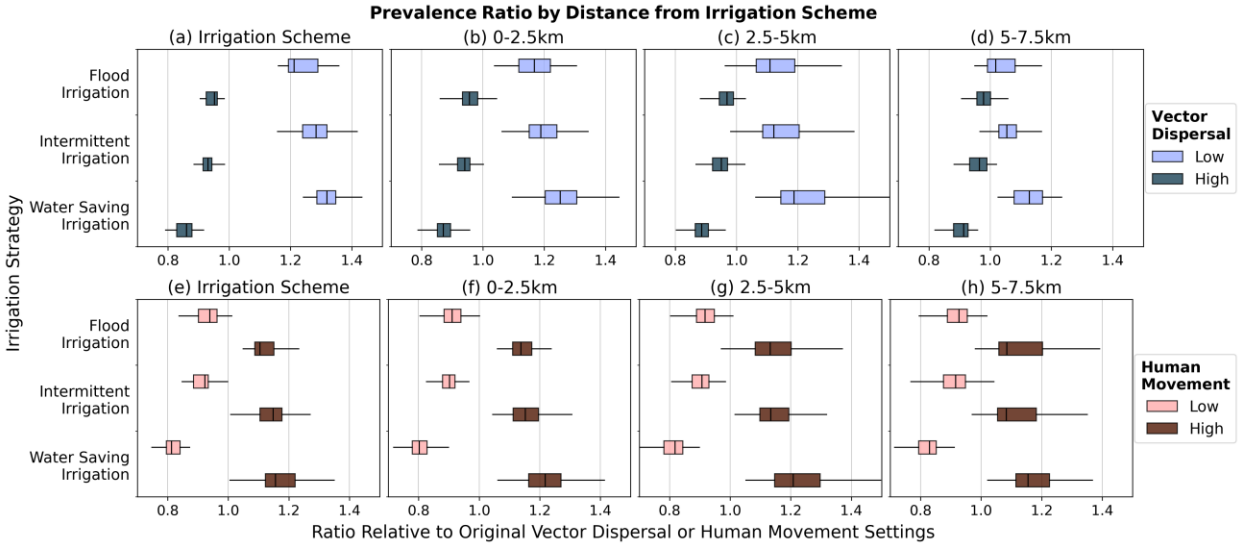

Figure 9. Ratio of mean annual prevalence relative to original (medium) human movement and vector dispersal setting by distance from the irrigation scheme for (a-d) varying vector dispersal scenarios and (e-h) varying human movement scenarios. The ratio was calculated for each irrigation strategy.

4 Discussion

4.1 Implications for water management and vector control

Expanding irrigation coverage in Homa Bay from 50% to 100% resulted in a nearly twofold increase in larval habitat area, with corresponding increases of 76% in EIR and 52% in malaria prevalence. These findings underscore the public health trade-offs that can accompany efforts to enhance agricultural resilience and stabilize yields through expanded water access. However, our results suggest that these impacts can be substantially mitigated by transitioning from conventional flood irrigation to more efficient water management strategies. Specifically, applying intermittent irrigation alone reduced habitat and transmission metrics by up to 23%, while combining it with drip irrigation in the water saving irrigation scenario cut these metrics by roughly half, ranging from 44% to 55% relative to conventional flooding. These reductions were most pronounced during the dry season, when irrigation becomes the primary driver of surface water pooling. Our findings are consistent with prior studies showing that intermittent irrigation introduces dry intervals that effectively interrupt mosquito breeding (Keiser et al., 2002; Mutero et al., 2000), while drip systems minimize surface water accumulation, thereby reducing the formation of larval habitats (Assefa et al., 2018; Maisiri et al., 2005).

A key insight from this study is that the timing and spatial distribution of water use appear to be more influential than the total volume of irrigation applied. Although the staple crop scenario required the greatest total volume of water, it did not result in the highest transmission metrics. Total irrigation volume alone may not be the primary driver of malaria risk; rather, the interaction between irrigation schedules and local hydrology is more important. For example, since rice cultivation in our model coincided with the long rainy season, when soils were already saturated, additional irrigation contributed minimally to further habitat expansion. This indicates that rice production, a critical pillar of food security, can be implemented in ways that do not necessarily exacerbate malaria risk, particularly when managed in natural floodplains during the wet season. Conversely, the cash crop scenario generated higher transmission risk by allocating water to non-flooded zones where habitat availability remained highly sensitive to irrigation inputs.

The sensitivity of these non-flooded and short-term flooded zones carries important implications for the practical management of irrigation initiatives. While our results demonstrate the potential benefits of the water saving irrigation scenario, successful field implementation of intermittent and drip irrigation requires aligning irrigation schedules with crop water requirements or soil moisture levels. In many sub-Saharan African contexts, however, farmers often apply irrigation based on immediate water availability or individual preference rather than coordinated, real-time crop demands (Munyaradzi et al., 2022; Nakawuka et al., 2018; Wanyama et al., 2024). Such ad hoc and poorly timed applications frequently produce uneven water distribution, leading to localized pooling in flat or poorly drained areas (Nakawuka et al., 2018). Stagnant water in these zones can sustain vector breeding and elevate transmission risk. Addressing these challenges requires investments in farmer training, monitoring tools, and institutional support to strengthen irrigation decision-making and improve water-use efficiency (Mdemu et al., 2020; Stirzaker et al., 2017).

Ultimately, these insights emphasize the importance of incorporating environmental management into broader malaria vector control strategies. While current efforts primarily rely on LLINs and IRS, these tools alone may be insufficient in landscapes where irrigation sustains year-round transmission (Tusting et al., 2013). Furthermore, the growing threat of insecticide resistance has renewed the need for complementary approaches (World Health Organization, 2023). Efficient irrigation methods, such as intermittent and drip systems, offer a dual benefit by supporting agricultural productivity and reducing vector breeding capacity. While challenges regarding farmer adoption, system infrastructure requirements, and financial accessibility remain (Nakawuka et al., 2018; Talukdar et al., 2023), aligning agricultural sustainability with health outcomes will be essential for effective malaria prevention in areas undergoing agricultural expansion (Keiser et al., 2005).

4.2 Spatial structure of malaria risk in irrigated landscapes

Irrigation strongly structures the spatial patterns of malaria transmission. Our results show a spatial gradient in both adult vector density and malaria prevalence, with the highest values near the irrigation scheme and decreasing with distance. Adult vector density declined relatively uniformly, whereas malaria prevalence showed greater local variability, likely reflecting differences in human population density. This pattern is consistent with field observations from the same region (Ondeto et al., 2022; Zhou et al., 2022) and with studies from other irrigation schemes reporting elevated malaria transmission near irrigated fields. For example, higher *Anopheles* density and EIR have been documented in rice and sugarcane plantations in Ethiopia compared to nearby non-irrigated areas (Haileselassie et al., 2021; Jaleta et al., 2013). Similarly, a spatiotemporal model of a smallholder irrigation scheme in Malawi suggested that adult *Anopheles* densities would likely be higher in households near irrigation infrastructure and decline exponentially with distance from irrigated areas (Frake et al., 2020).

Different irrigation strategies modified these spatial patterns by altering larval habitat availability and persistence. In the water saving irrigation scenario, the model shows localized clusters of higher malaria prevalence within the irrigated area (Figure 8f). This pattern likely resulted from reduced surface ponding, which limited the formation of breeding habitats and concentrates larval development in specific parts of the scheme. These conditions have important implications for vector control. When transmission becomes spatially clustered, interventions can be more effectively targeted to high-risk areas. In such settings, larval source management, including larviciding, becomes more feasible because breeding sites are fewer and spatially concentrated. Targeted indoor residual spraying can also be more efficiently implemented, as control efforts can be prioritized in areas with higher transmission intensity. In contrast, flood irrigation generates more widespread habitat distribution, which reduces the practicality of spatially targeted interventions and increases reliance on area-wide control approaches. These results highlight that irrigation design can influence not only water use but also the spatial pattern of malaria risk and the feasibility of targeted control strategies.

At larger spatial scales, mosquito dispersal further shaped the distribution of adult vector populations between the irrigation scheme and surrounding areas. The low vector dispersal scenario concentrated mosquitoes within irrigated zones relative to the medium setting, whereas the high vector dispersal scenario redistributed them into more distant

locations. The magnitude of these changes depended on the irrigation strategy, which determined the degree of spatial heterogeneity in habitat availability across the landscape. Under flood irrigation, dispersal led to larger shifts in vector density across zones, while the effects were progressively smaller under intermittent and water saving irrigation scenarios. This pattern reflected the high density of breeding habitats within flood-irrigated areas, which acted as strong source regions relative to their surroundings. Under the high vector dispersal scenario, mosquitoes moved from these high-capacity habitats into areas with fewer breeding opportunities, resulting in more pronounced changes in density. Similar dispersal-driven redistribution has been observed in a spatial mosquito model where breeding sites differ substantially in carrying capacity, with higher dispersal leading to depopulation of highly productive patches (McCormack et al., 2019).

In contrast to the patterns observed for vector density, malaria prevalence responded more strongly to mosquito dispersal and human movement under water saving irrigation than under less efficient irrigation strategies. Under flood irrigation, consistently high mosquito abundance sustained frequent mosquito-human contact, so prevalence remained relatively stable even when the movement between zones varied. In water saving irrigation scenario, lower mosquito abundance reduced overall transmission intensity. Under these conditions, changes in mosquito dispersal or human movement had a greater influence on mosquito-human contact, leading to larger shifts in malaria prevalence across zones. This interpretation is consistent with a study showing that malaria transmission efficiency is highest in low-intensity settings and declines nonlinearly with greater exposure to infectious bites (D. L. Smith et al., 2010).

These results highlight the importance of considering movement processes when evaluating malaria risk in irrigated landscapes. Mosquito dispersal influences how adult vectors spread from concentrated breeding habitats within irrigation schemes, while human travel can connect areas with different levels of transmission. The model results suggest that the epidemiological consequences of these processes depend on the underlying irrigation environment. Spatially explicit models therefore provide a useful framework for understanding how habitat distribution and movement processes interact to structure malaria transmission across irrigated and surrounding areas (Bomblies, 2014; D. L. Smith et al., 2004).

4.3 Limitations

Several simplifying assumptions were made in this study, which may introduce uncertainty in the model outputs.

First, we used ParFlow-CLM to simulate potential aquatic habitats, which did not necessarily correspond to habitats that support mosquito larvae. Larval development depends on additional factors such as water quality, vegetation, and predation, which were not explicitly represented in our model. To address this, we used field survey data to estimate larval capacity and constrain larval production within the simulated habitats. However, these capacity values were assigned based on broad habitat categories (e.g., temporary, semi-permanent, or permanent) and lacked temporal variability, limiting the model's ability to capture where and when larvae are likely to occur within these aquatic areas. Integrating remote sensing products

with hydrologic simulations could improve the identification of larval habitats by incorporating environmental information beyond water presence.

Second, irrigation was represented using an idealized scheduling scheme. In ParFlow-CLM, water was applied when soil saturation dropped below a threshold, assuming irrigation was timed to meet crop water demand. In practice, farmers in the Oluch irrigation scheme often rely on individual judgment, leading to variability in both timing and application amounts. This simplification likely resulted in overestimated and overly uniform irrigation patterns. In addition, the model resolution was too coarse to explicitly represent drip irrigation. We approximated this by separating irrigated areas into wet and dry pixels, but translating plot-scale wetting patterns to the model grid could still introduce uncertainties (Pool et al., 2021). Incorporating field-observed irrigation schedules and higher-resolution modeling frameworks would better capture farmer behavior and the spatial heterogeneity of irrigation practices.

Finally, human and mosquito mobility were simplified. Human movement was represented using a radiation model based on population and distance, which did not capture local movement patterns or key drivers such as social behavior and environmental constraints (Camargo et al., 2019; Riley et al., 2015; Sallah et al., 2017). Mosquito dispersal was modeled as a random walk and did not account for directional responses toward hosts, breeding sites, or wind (Gu & Novak, 2009; Huestis et al., 2019). The model also excluded landscape features such as roads, buildings, and vegetation that could influence the dispersal (Francisco & Watanabe, 2024; Hemme et al., 2010; Hemming-Schroeder et al., 2020). Using data-informed human mobility (e.g., mobile phone or survey data) and more realistic mosquito movement models that incorporate behavioral responses and environmental drivers (Cummins et al., 2012) would improve the representation of spatial transmission patterns.

5 Conclusions

This study evaluates the effects of cropping practices, irrigation strategies, and human and mosquito mobility on malaria transmission in an irrigation scheme in western Kenya. By linking hydrological processes with disease dynamics, it provides a mechanistic understanding of the role of agricultural water management in shaping vector habitats and transmission risk.

Our results show that improving irrigation practices reduced mosquito habitat availability, EIR, and malaria prevalence by limiting surface water accumulation. It also led to more spatially concentrated transmission, making targeted vector control more practical. Under these conditions, mobility posed a greater influence on malaria prevalence, as local reductions in breeding habitats increased the relative importance of mosquito dispersal and human movement in transmission patterns.

Across cropping scenarios, water intensive crops such as rice did not result in higher malaria transmission than less water intensive alternatives. This indicates that irrigation volume alone does not drive vector proliferation; rather, the timing and spatial distribution of water use play a more important role in determining conditions that support mosquito development. This suggests that rice production can support food security without necessarily increasing malaria transmission.

As irrigation expands across sub-Saharan Africa, managing its unintended health impacts becomes increasingly important. This study highlights the need to better align agricultural water management with malaria control by accounting for how irrigation design influences vector ecology and transmission dynamics. Future work should focus on validating these results with field observations, exploring a broader range of cropping and irrigation configurations, and integrating socio-economic factors that influence farmer decision-making. Such efforts are essential for developing irrigation systems that support both food production and public health.

Acknowledgments

This work was supported by the National Institutes of Health (R21 AI174183 and U19 AI129326). The funders had no role in the study design, data collection and analysis, decision to publish, or preparation of the manuscript. We thank the project management and coordination office of the Kimira-Oluch Smallholder Farm Improvement Project for providing project reports that informed the cropping practices and irrigation configurations used in our model. We also gratefully acknowledge the field team and staff of the sub-Saharan Africa International Center for Malaria Research for their contributions of field data and contextual insights that supported this study. In addition, we thank Caitlin Bever, Prashanth Selvaraj, and Daniel Bridenbecker at the Institute for Disease Modeling, Bill & Melinda Gates Foundation, for their invaluable technical support. The authors declare no conflicts of interest related to this study.

Open Research

The simulation softwares used in this research, ParFlow-CLM and EMOD, are available at Zenodo (S. Smith et al., 2023) and Github (Institute for Disease Modeling, 2025), respectively. Precipitation data used as input for ParFlow-CLM can be obtained from the Data Portal of the Center for Hydrometeorology and Remote Sensing (Nguyen et al., 2019). Other climate input data were retrieved from the Climate Data Store (Hersbach et al., 2023). Surface elevation data are available from the Copernicus Data Space Ecosystem (D. Kovács et al., 2026). Land cover data were sourced from the Esri Sentinel-2 Land Cover Explorer (Esri, 2024) and soil data were downloaded from the SoilGrid database (ISRIC-World Soil Information, 2023). All input files, simulation scripts, and calibration data used in the EMOD simulations are available on Zenodo (Jiang et al., 2025).

References

Adler, R. F., Huffman, G. J., Chang, A., Ferraro, R., Xie, P.-P., Janowiak, J., et al. (2003). The version-2 global precipitation climatology project (GPCP) monthly precipitation analysis (1979–present). *Journal of hydrometeorology, 4*(6), 1147-1167.

Airbus, D. (2020). Copernicus dem copernicus digital elevation model validation report. *Airbus Defence and Space—Intelligence: Potsdam, Germany*.

Allen, R. G., Pereira, L. S., Raes, D., & Smith, M. (1998). FAO Irrigation and drainage paper No. 56. *Rome: food and agriculture organization of the United Nations, 56*(97), e156.

Ashby, S. F., & Falgout, R. D. (1996). A parallel multigrid preconditioned conjugate gradient algorithm for groundwater flow simulations. *Nuclear science and engineering, 124*(1), 145-159.

Assefa, T., Jha, M., Reyes, M., & Worqlul, A. W. (2018). Modeling the impacts of conservation agriculture with a drip irrigation system on the hydrology and water management in Sub-Saharan Africa. *Sustainability, 10*(12), 4763.

Atieli, H. E., Zhou, G., Zhong, D., Wang, X., Lee, M.-c., Yaro, A. S., et al. (2023). Wind-assisted high-altitude dispersal of mosquitoes and other insects in East Africa. *Journal of Medical Entomology, 60*(4), 698-707.

Aurenhammer, F. (1991). Voronoi diagrams—a survey of a fundamental geometric data structure. *ACM computing surveys (CSUR), 23*(3), 345-405.

Bershteyn, A., Gerardin, J., Bridenbecker, D., Lorton, C. W., Bloedow, J., Baker, R. S., et al. (2018). Implementation and applications of EMOD, an individual-based multi-disease modeling platform. *Pathogens and disease, 76*(5), fty059.

Bomblies, A. (2014). Agent-based modeling of malaria vectors: the importance of spatial simulation. *Parasites & vectors, 7*(1), 308.

Boyce, M. S., Vernier, P. R., Nielsen, S. E., & Schmiegelow, F. K. (2002). Evaluating resource selection functions. *Ecological modelling, 157*(2-3), 281-300.

Brodsky, I. (2018). H3: Uber's hexagonal hierarchical spatial index. *Available from Uber Engineering website: https://eng. uber. com/h3/[22 June 2019], 30*.

Camargo, C. Q., Bright, J., & Hale, S. A. (2019). Diagnosing the performance of human mobility models at small spatial scales using volunteered geographical information. *Royal Society open science, 6*(11), 191034.

Camlin, C. S., Akullian, A., Neilands, T. B., Getahun, M., Bershteyn, A., Ssali, S., et al. (2019). Gendered dimensions of population mobility associated with HIV across three epidemics in rural Eastern Africa. *Health & place, 57*, 339-351.

Chan, K., Bottomley, C., Saito, K., Lines, J., & Tusting, L. S. (2022). The control of malaria vectors in rice fields: a systematic review and meta-analysis. *Scientific reports, 12*(1), 19694.

Cousens, R., Dytham, C., & Law, R. (2008). *Dispersal in plants: a population perspective*: Oxford University Press.

Cummins, B., Cortez, R., Foppa, I. M., Walbeck, J., & Hyman, J. M. (2012). A spatial model of mosquito host-seeking behavior. *PLoS computational biology, 8*(5), e1002500.

D. Kovács, D., Musial, J., Bojanowski, J., Clarijs, D., de la Mar, J., & Zlinszky, A. (2026). Copernicus Data Space Ecosystem establishes public cloud processing for earth observation data. *Scientific data*.

Dai, Y., Zeng, X., Dickinson, R. E., Baker, I., Bonan, G. B., Bosilovich, M. G., et al. (2003). The common land model. *Bulletin of the American Meteorological Society, 84*(8), 1013-1024.

De Lellis, P., Ruiz Marín, M., & Porfiri, M. (2021). Modeling human migration under environmental change: a case study of the effect of sea level rise in Bangladesh. *Earth's Future, 9*(4), e2020EF001931.

Djègbè, I., Zinsou, M., Dovonou, E. F., Tchigossou, G., Soglo, M., Adéoti, R., et al. (2020). Minimal tillage and intermittent flooding farming systems show a potential reduction in the proliferation of Anopheles mosquito larvae in a rice field in Malanville, Northern Benin. *Malaria Journal, 19*, 1-10.

Eckhoff, P. A. (2011). A malaria transmission-directed model of mosquito life cycle and ecology. *Malaria Journal, 10*, 1-17.

Eckhoff, P. A. (2012a). Malaria parasite diversity and transmission intensity affect development of parasitological immunity in a mathematical model. *Malaria Journal, 11*, 1-14.

Eckhoff, P. A. (2012b). P. falciparum infection durations and infectiousness are shaped by antigenic variation and innate and adaptive host immunity in a mathematical model.

Eckhoff, P. A. (2013). Mathematical models of within-host and transmission dynamics to determine effects of malaria interventions in a variety of transmission settings. *The American journal of tropical medicine and hygiene, 88*(5), 817.

Esri. (2024). Sentinel-2 Land Cover Explorer. Retrieved from https://livingatlas.arcgis.com/landcoverexplorer/

Fang, B., Lakshmi, V., & Zhang, R. (2024). Validation of downscaled 1-km SMOS and SMAP soil moisture data in 2010–2021. *Vadose Zone Journal, 23*(2), e20305.

Food and Agriculture Organization. (2020). *WaPOR database methodology: version 2 release, April 2020*. Rome, Italy: FAO.

Food and Agriculture Organization. (2021). *Crop Calendar - Information Tool for Crop Production*. United Nations. Retrieved from https://cropcalendar.apps.fao.org/#/home

Frake, A. N., Namaona, W., Walker, E. D., & Messina, J. P. (2020). Estimating spatio-temporal distributions of mosquito breeding pools in irrigated agricultural schemes: a case study at the Bwanje Valley Irrigation Scheme. *Malaria Journal, 19*, 1-21.

Frake, A. N., Peter, B. G., Chipula, G., & Messina, J. P. (2024). Spatial targeting of irrigation development and water resource management to mitigate vector-borne disease. *Journal of Environmental Management, 363*, 121398.

Francisco, M. E., & Watanabe, K. (2024). Innovative house structures for malaria vector control in Nampula district, Mozambique: assessing mosquito entry prevention, indoor comfort, and community acceptance. *Frontiers in Public Health, 12*, 1404493.

Frenken, K. (2005). *Irrigation in Africa in figures: AQUASTAT survey, 2005* (Vol. 29): Food & Agriculture Org.

GFA Terra Systems, CAS Consultants, & CES Concultants. (2005). *Kimira-Oluch Smallholder Irrigation Development Study Final Design Report*. Republic of Kenya. Kenya.

GFA Terra Systems, CES, & CAS. (2003). *Kimira Oluch Smallholder Irrigation Development Study Final Design Report*. Republic of Kenya. Kenya.

Gianotti, R. L., Bomblies, A., & Eltahir, E. A. (2009). Hydrologic modeling to screen potential environmental management methods for malaria vector control in Niger. *Water resources research, 45*(8).

Gillison, A. N. (2016). Vegetation functional types and traits at multiple scales. In *Vegetation structure and function at multiple spatial, temporal and conceptual scales* (pp. 53-97): Springer.

Gleeson, T., Moosdorf, N., Hartmann, J., & van Beek, L. v. (2014). A glimpse beneath earth's surface: GLobal HYdrogeology MaPS (GLHYMPS) of permeability and porosity. *Geophysical Research Letters, 41*(11), 3891-3898.

Gracia-de-Rentería, P., Nechifor, V., & Ferrari, E. (2024). Capturing the drivers of crop water footprints in Africa and its spatial patterns. *Water Resources and Economics, 47*, 100248.

Gu, W., & Novak, R. J. (2009). Agent-based modelling of mosquito foraging behaviour for malaria control. *Transactions of the Royal Society of Tropical Medicine and Hygiene, 103*(11), 1105-1112.

Gupta, S., Hengl, T., Lehmann, P., Bonetti, S., & Or, D. (2020). SoilKsatDB: global soil saturated hydraulic conductivity measurements for geoscience applications. *Earth System Science Data Discussions, 2020*, 1-26.

Haileselassie, W., Zemene, E., Lee, M.-C., Zhong, D., Zhou, G., Taye, B., et al. (2021). The effect of irrigation on malaria vector bionomics and transmission intensity in western Ethiopia. *Parasites & vectors, 14*, 1-11.

Hemme, R. R., Thomas, C. L., Chadee, D. D., & Severson, D. W. (2010). Influence of urban landscapes on population dynamics in a short-distance migrant mosquito: evidence for the dengue vector Aedes aegypti. *PLoS neglected tropical diseases, 4*(3), e634.

Hemming-Schroeder, E., Zhong, D., Machani, M., Nguyen, H., Thong, S., Kahindi, S., et al. (2020). Ecological drivers of genetic connectivity for African malaria vectors Anopheles gambiae and An. arabiensis. *Scientific reports, 10*(1), 19946.

Hengl, T., Mendes de Jesus, J., Heuvelink, G. B., Ruiperez Gonzalez, M., Kilibarda, M., Blagotić, A., et al. (2017). SoilGrids250m: Global gridded soil information based on machine learning. *PloS one, 12*(2), e0169748.

Hersbach, H., Bell, B., Berrisford, P., Biavati, G., Horányi, A., Muñoz Sabater, J., et al. (2023). ERA5 hourly data on single levels from 1940 to present, Copernicus Climate Change Service (C3S) Climate Data Store (CDS)[data set]. In.

Higginbottom, T. P., Adhikari, R., Dimova, R., Redicker, S., & Foster, T. (2021). Performance of large-scale irrigation projects in sub-Saharan Africa. *Nature Sustainability, 4*(6), 501-508.

Hirzel, A. H., Le Lay, G., Helfer, V., Randin, C., & Guisan, A. (2006). Evaluating the ability of habitat suitability models to predict species presences. *Ecological modelling, 199*(2), 142-152.

Huestis, D. L., Dao, A., Diallo, M., Sanogo, Z. L., Samake, D., Yaro, A. S., et al. (2019). Windborne long-distance migration of malaria mosquitoes in the Sahel. *Nature, 574*(7778), 404-408.

Institute for Disease Modeling. (2025). EMOD-Hub/EMOD: EMOD Version 2.22 (v2.22) [Software]. Retrieved from https://github.com/EMOD-Hub/EMOD

ISRIC-World Soil Information. (2023). SoilGrids: Global gridded soil information system. Retrieved from https://soilgrids.org/

Jaleta, K. T., Hill, S. R., Seyoum, E., Balkew, M., Gebre-Michael, T., Ignell, R., & Tekie, H. (2013). Agro-ecosystems impact malaria prevalence: large-scale irrigation drives vector population in western Ethiopia. *Malaria Journal, 12*, 1-11.

Janko, M. M., Irish, S. R., Reich, B. J., Peterson, M., Doctor, S. M., Mwandagalirwa, M. K., et al. (2018). The links between agriculture, Anopheles mosquitoes, and malaria risk in children younger than 5 years in the Democratic Republic of the Congo: a population-based, cross-sectional, spatial study. *The Lancet Planetary Health, 2*(2), e74-e82.

Jiang, A.-L., Hsu, K., Sanders, B. F., & Sorooshian, S. (2023). Topographic hydro-conditioning to resolve surface depression storage and ponding in a fully distributed hydrologic model. *Advances in water resources, 176*, 104449.

Jiang, A.-L., Lee, M.-C., Selvaraj, P., Degefa, T., Getachew, H., Merga, H., et al. (2023). Investigating the impact of irrigation on malaria vector larval habitats and transmission using a hydrology-based model. *GeoHealth, 7*(12), e2023GH000868.

Jiang, A.-L., Lee, M.-C., Yan, G., & Hsu, K. (2025). Supplemental data for "Hydrology-Based Assessment of Malaria Transmission Under Cropping and Irrigation Practices in Western Kenya" [Dataset]. Zenodo. https://doi.org/10.5281/zenodo.15802998.

Jiang, A.-L., Lee, M.-C., Zhou, G., Zhong, D., Hawaria, D., Kibret, S., et al. (2021). Predicting distribution of malaria vector larval habitats in Ethiopia by integrating distributed hydrologic modeling with remotely sensed data. *Scientific reports, 11*(1), 10150.

Jones, J. E., & Woodward, C. S. (2001). Newton–Krylov-multigrid solvers for large-scale, highly heterogeneous, variably saturated flow problems. *Advances in water resources, 24*(7), 763-774.

Kanda, E. K., & Lutta, V. O. (2022). The status and challenges of a modern irrigation system in Kenya: A systematic review. *Irrigation and Drainage, 71*, 27-38.

Karpouzoglou, T., & Barron, J. (2014). A global and regional perspective of rainwater harvesting in sub-Saharan Africa's rainfed farming systems. *Physics and Chemistry of the Earth, Parts A/B/C, 72*, 43-53.

Karra, K., Kontgis, C., Statman-Weil, Z., Mazzariello, J. C., Mathis, M., & Brumby, S. P. (2021, 11-16 July 2021). *Global land use / land cover with Sentinel 2 and deep learning.* Paper presented at the 2021 IEEE International Geoscience and Remote Sensing Symposium IGARSS.

Keiser, J., De Castro, M. C., Maltese, M. F., Bos, R., Tanner, M., Singer, B. H., & Utzinger, J. (2005). Effect of irrigation and large dams on the burden of malaria on a global and regional scale. *American Journal of Tropical Medicine and Hygiene, 72*(4), 392-406.

Keiser, J., Utzinger, J., & Singer, B. H. (2002). The potential of intermittent irrigation for increasing rice yields, lowering water consumption, reducing methane emissions, and controlling malaria in African rice fields. *Journal of the American Mosquito Control Association, 18*(4), 329-340.

Kibret, S., Lautze, J., McCartney, M., Wilson, G. G., & Nhamo, L. (2015). Malaria impact of large dams in sub-Saharan Africa: maps, estimates and predictions. *Malaria Journal, 14*, 1-12.

Kibret, S., Ryder, D., Wilson, G. G., & Kumar, L. (2019). Modeling reservoir management for malaria control in Ethiopia. *Scientific reports, 9*(1), 18075.

Kollet, S. J., & Maxwell, R. M. (2006). Integrated surface–groundwater flow modeling: A free-surface overland flow boundary condition in a parallel groundwater flow model. *Advances in water resources, 29*(7), 945-958.

Lakshmi, V., & Fang, B. (2023). SMAP-Derived 1-km downscaled surface soil moisture product, Version 1. *Boulder, Colorado USA. NASA National Snow and Ice Data Center Distributed Active Archive Center*.

Leung, S., Windbichler, N., Wenger, E. A., Bever, C. A., & Selvaraj, P. (2022). Population replacement gene drive characteristics for malaria elimination in a range of seasonal transmission settings: a modelling study. *Malaria Journal, 21*(1), 226.

Lutambi, A. M., Penny, M. A., Smith, T., & Chitnis, N. (2013). Mathematical modelling of mosquito dispersal in a heterogeneous environment. *Mathematical biosciences, 241*(2), 198-216.

Maisiri, N., Senzanje, A., Rockstrom, J., & Twomlow, S. (2005). On farm evaluation of the effect of low cost drip irrigation on water and crop productivity compared to conventional surface irrigation system. *Physics and Chemistry of the Earth, Parts A/B/C, 30*(11-16), 783-791.

Makone, S. M., Basweti, E. A., & Bunyatta, D. K. (2021). Effects of irrigation systems on farming practices: evidence from Oluch-Kimira Scheme, Homa Bay County, Kenya. *Asian J Adv Res Rep, 15*, 26-35.

Maxwell, R. M. (2013). A terrain-following grid transform and preconditioner for parallel, large-scale, integrated hydrologic modeling. *Advances in water resources, 53*, 109-117.

Maxwell, R. M., & Kollet, S. J. (2008). Interdependence of groundwater dynamics and land-energy feedbacks under climate change. *Nature Geoscience, 1*(10), 665-669.

Mboera, L. E., Senkoro, K. P., Mayala, B. K., Rumisha, S. F., Rwegoshora, R. T., Mlozi, M. R., & Shayo, E. H. (2010). Spatio-temporal variation in malaria transmission intensity in five agro-ecosystems in Mvomero district, Tanzania. *Geospatial health, 4*(2), 167-178.

McCormack, C. P., Ghani, A. C., & Ferguson, N. M. (2019). Fine-scale modelling finds that breeding site fragmentation can reduce mosquito population persistence. *Communications Biology, 2*(1), 273.

Mdemu, M., Kissoly, L., Bjornlund, H., Kimaro, E., Christen, E., van Rooyen, A., et al. (2020). The role of soil water monitoring tools and agricultural innovation platforms in improving food security and income of farmers in smallholder irrigation schemes in Tanzania. *International Journal of Water Resources Development, 36*(sup1), S148-S170.

Merrey, D. J., McCornick, P. G., & Nance, M. C. (2017). Pathways to increasing farmer-led investments in sustainable agricultural water management in sub-Saharan Africa.

Meta. (2025). High Resolution Population Density Maps. Retrieved from https://dataforgood.facebook.com/dfg/tools/high-resolution-population-density-maps

Munyaradzi, M., Hapanyengwi, G., Masocha, M., Mutandwa, E., Raeth, P., Nyambo, B., et al. (2022). Precision Irrigation Scheduling Based on Wireless Soil Moisture Sensors to Improve Water Use Efficiency and Yield for Winter Wheat in Sub-Saharan Africa. *Advances in Agriculture, 2022*(1), 8820764.

Mutero, C. M., Blank, H., Konradsen, F., & Van Der Hoek, W. (2000). Water management for controlling the breeding of Anopheles mosquitoes in rice irrigation schemes in Kenya. *Acta tropica, 76*(3), 253-263.

Nakawuka, P., Langan, S., Schmitter, P., & Barron, J. (2018). A review of trends, constraints and opportunities of smallholder irrigation in East Africa. *Global food security, 17*, 196-212.

Nguyen, P., Ombadi, M., Gorooh, V. A., Shearer, E. J., Sadeghi, M., Sorooshian, S., et al. (2020). Persiann dynamic infrared–rain rate (PDIR-now): A near-real-time, quasi-global satellite precipitation dataset. *Journal of hydrometeorology, 21*(12), 2893-2906.

Nguyen, P., Shearer, E. J., Tran, H., Ombadi, M., Hayatbini, N., Palacios, T., et al. (2019). The CHRS Data Portal, an easily accessible public repository for PERSIANN global satellite precipitation data. *Scientific data, 6*(1), 1-10.

Ntabaliba, W., Vavassori, L., Stica, C., Makungwa, N., Odufuwa, O. G., Swai, J. K., et al. (2023). Life expectancy of Anopheles funestus is double that of Anopheles arabiensis in southeast Tanzania based on mark-release-recapture method. *Scientific reports, 13*(1), 15775.

Omondi, C. J., Otambo, W. O., Odongo, D., Ochwedo, K. O., Otieno, A., Onyango, S. A., et al. (2022). Asymptomatic and submicroscopic Plasmodium infections in an area before and during integrated vector control in Homa Bay, western Kenya. *Malaria Journal, 21*(1), 272.

Omoro, J. (2018). Why a Sh6 billion irrigation project is wasting. *The Standard*. Retrieved from https://www.standardmedia.co.ke/article/2001273523/why-a-sh6-billion-irrigation-project-is-wasting-away

Ondeto, B. M., Wang, X., Atieli, H., Orondo, P. W., Ochwedo, K. O., Omondi, C. J., et al. (2022). Malaria vector bionomics and transmission in irrigated and non-irrigated sites in western Kenya. *Parasitology research, 121*(12), 3529-3545.

Onyango, A. (2023). Farmers' joy as irrigation project limps back to life. *FarmKenya*. Retrieved from https://www.standardmedia.co.ke/farmkenya/article/2001465642/farmers-joy-as-irrigation-project-limps-back-to-life

Orondo, P. W., Wang, X., Lee, M.-C., Nyanjom, S. G., Atieli, H., Ondeto, B. M., et al. (2023). Habitat diversity, stability, and productivity of malaria vectors in irrigated and nonirrigated ecosystems in western Kenya. *Journal of Medical Entomology, 60*(1), 202-212.

Osika, N. O., Onyango, L., & Ogindo, H. (2023). Climate related challenges faced by smallholder farmers in Kimira Oluch Smallholder Irrigation Project in Homabay County, Kenya. *IOSR Journal Of Humanities And Social Science, 28*(2), 21-28.

Ouma, M. A., Ouma, L. O., Ombati, J. M., & Onyango, C. A. (2024). A cost benefits analysis of the adoption of system of rice intensification: Evidence from smallholder rice farmers within an innovation platform in Oluch irrigation scheme, Kenya. *PloS one, 19*(1), e0290759.

Patz, J. A., Graczyk, T. K., Geller, N., & Vittor, A. Y. (2000). Effects of environmental change on emerging parasitic diseases. *International journal for parasitology, 30*(12-13), 1395-1405.

Pindolia, D. K., Garcia, A. J., Wesolowski, A., Smith, D. L., Buckee, C. O., Noor, A. M., et al. (2012). Human movement data for malaria control and elimination strategic planning. *Malaria Journal, 11*(1), 205.

Poméon, T., Wagner, N., Furusho, C., Kollet, S., & Reinoso-Rondinel, R. (2020). Performance of a PDE-based hydrologic model in a flash flood modeling framework in sparsely-gauged catchments. *Water, 12*(8), 2157.

Pool, S., Francés, F., Garcia-Prats, A., Puertes, C., Pulido-Velazquez, M., Sanchis-Ibor, C., et al. (2021). Hydrological modeling of the effect of the transition from flood to drip irrigation on groundwater recharge using multi-objective calibration. *Water resources research, 57*(8), e2021WR029677.

Reis, J., Culver, T. B., McCartney, M., Lautze, J., & Kibret, S. (2011). Water resources implications of integrating malaria control into the operation of an Ethiopian dam. *Water resources research, 47*(9).

Richards, L. A. (1931). Capillary conduction of liquids through porous mediums. *physics, 1*(5), 318-333.

Riley, S., Eames, K., Isham, V., Mollison, D., & Trapman, P. (2015). Five challenges for spatial epidemic models. *Epidemics, 10*, 68-71.

Ruder, S. (2016). An overview of gradient descent optimization algorithms. *arXiv preprint arXiv:1609.04747*.

Saadi, M., Furusho-Percot, C., Belleflamme, A., Chen, J.-Y., Trömel, S., & Kollet, S. (2022). How uncertain are precipitation and peakflow estimates for the July 2021 flooding event? *Natural Hazards and Earth System Sciences Discussions, 2022*, 1-28.

Sallah, K., Giorgi, R., Bengtsson, L., Lu, X., Wetter, E., Adrien, P., et al. (2017). Mathematical models for predicting human mobility in the context of infectious disease spread: introducing the impedance model. *International journal of health geographics, 16*, 1-11.

Simini, F., González, M. C., Maritan, A., & Barabási, A.-L. (2012). A universal model for mobility and migration patterns. *Nature, 484*(7392), 96-100.

Smith, D. L., Drakeley, C. J., Chiyaka, C., & Hay, S. I. (2010). A quantitative analysis of transmission efficiency versus intensity for malaria. *Nature communications, 1*(1), 108.

Smith, D. L., Dushoff, J., & McKenzie, F. E. (2004). The risk of a mosquito-borne infectionin a heterogeneous environment. *PLoS biology, 2*(11), e368.

Smith, S., Ferguson, I., Engdahl, N., Gasper, F., Chennault, C., Avery, P., et al. (2023). parflow/parflow: ParFlow Version 3.12.0 (v3.12.0) [Software]. Zenodo. https://doi.org/10.5281/zenodo.7510554.

Stirzaker, R., Mbakwe, I., & Mziray, N. R. (2017). A soil water and solute learning system for small-scale irrigators in Africa. *International Journal of Water Resources Development, 33*(5), 788-803.

Talukdar, O., Bhattacharya, S. S., & Gogoi, N. (2023). Alternate wet and dry irrigation technology as a sustainable water management and disease vector control tool. *Environmental Quality Management, 33*(1), 23-42.

Thomas, C. J., Cross, D. E., & Bøgh, C. (2013). Landscape movements of Anopheles gambiae malaria vector mosquitoes in rural Gambia. *PloS one, 8*(7), e68679.

Tusting, L. S., Thwing, J., Sinclair, D., Fillinger, U., Gimnig, J., Bonner, K. E., et al. (2013). Mosquito larval source management for controlling malaria. *Cochrane database of systematic reviews*(8).

Verdonschot, P. F., & Besse-Lototskaya, A. A. (2014). Flight distance of mosquitoes (Culicidae): a metadata analysis to support the management of barrier zones around rewetted and newly constructed wetlands. *Limnologica, 45*, 69-79.

Walker, K., & Lynch, M. (2007). Contributions of Anopheles larval control to malaria suppression in tropical Africa: review of achievements and potential. *Medical and veterinary entomology, 21*(1), 2-21.

Wanyama, J., Bwambale, E., & Nakawuka, P. (2024). Comparative performance assessment of pilot irrigation schemes in Uganda. *Heliyon, 10*(10).

World Health Organization. (2023). *WHO Guidelines for malaria*: Geneva: World Health Organization.

World Health Organization. (2024). *World malaria report 2024*: Geneva: World Health Organization.

Xie, H., Perez, N., Anderson, W., Ringler, C., & You, L. (2020). Can Sub-Saharan Africa feed itself? The role of irrigation development in the region's drylands for food security. In *Virtual Water* (pp. 80-98): Routledge.

Zhou, G., Hemming-Schroeder, E., Jeang, B., Wang, X., Zhong, D., Lee, M.-C., et al. (2022). Irrigation-induced environmental changes sustain malaria transmission and compromise intervention effectiveness. *The Journal of infectious diseases, 226*(9), 1657-1666.